TECHNICAL NOTE • OPEN ACCESS

Closed-loop corrective beam shaping for laser processing of curved surfaces

View the article online for updates and enhancements.

IOP ebooks™

Bringing you innovative digital publishing with leading voices to create your essential collection of books in STEM research.

Start exploring the collection - download the first chapter of every title for free.

Technical Note

Closed-loop corrective beam shaping for laser processing of curved surfaces

Daniel J Heath[1] , **Benita S Mackay**[1] , **James A Grant-Jacob**[1], **Yunhui Xie**[1],
Richard O C Oreffo[2], **Robert W Eason**[1] **and Ben Mills**[1]

[1] Optoelectronics Research Centre, University of Southampton, Southampton, SO17 1BJ,
United Kingdom
[2] Bone and Joint Research Group, Centre for Human Development, Stem Cells and Regeneration,
Institute of Developmental Sciences, University of Southampton, Southampton S016 6YD, United Kingdom

E-mail: djh2v07@soton.ac.uk

CrossMark

Abstract
Laser processing is a widely used contactless machining technique, with ultrashort pulses
affording the intensity to machine almost any material. However, micro-patterning over curved
surfaces can be difficult, as a fixed beam shape will necessarily be skewed when directed at
a non-orthogonal sample surface. Here, we show that this aberration can be compensated via
closed-loop adaptive beam shaping, via the use of a MEMS device (Texas Instruments Digital
Micromirror device) acting as an intensity spatial light modulator that is used to create a beam
intensity profile transformation that takes into account the local surface gradient of the sample.
The patterning of 18 μm diameter circular structures over a region of a 3.00 mm diameter
titanium sphere has been demonstrated. Inclinations of the surface normal of up to $\pi/2$ from
the vertical were tested, and the effective range was found to be up to $\pi/5$. The MEMs device
is also shown to be capable of providing a real-time and precise laser beam repositioning that
compensates for the errors in the movement stages.

Keywords: digital micromirror device, laser processing, laser beam shaping, micromachining

(Some figures may appear in colour only in the online journal)

1. Introduction

Laser machining offers the capability for precise and non-contact fabrication on length scales that span nanometers to meters [1, 2]. In particular, femtosecond laser micromachining offers a reduced heat-affected zone and higher resolution compared to longer-pulsed or continuous-wave (c.w.) sources [3]. Functionalisation of surfaces in this field has demonstrated many potential end uses. Super hydrophobic surfaces have shown applications in biocompatibility [4, 5], anti-icing [6], anti-corrosion [7] and drag reduction [8]. Micro-texturing of metals can enhance absorption in solar cells and stealth applications [9, 10]. Micro- and nano-structured surfaces displaying diffractive effects can even be used for purely decorative purposes [11, 12]. More extensive reviews of the literature have been made by others [13] but, in general, the various techniques rely on a known intensity profile to remain uniform across regions of interest on the sample, to produce regular material modifications. Machining over a curved surface, i.e. one that contains angles that are not orthogonal to the direction of the laser source, complicates the fulfilment of this requirement. The projection of a fixed beam-shape at varying local surface gradients on a sample will result in changing

skews and stretches to the machined structure profile, as in figure 1(a). In order to laser machine over non-orthogonal surfaces, the sample may be rotated in order to achieve a direct line-of-sight access to the sample. However, for some particularly complicated or curved surfaces, such as those with deep fissures (e.g. figure 1), direct access may not be possible, and clipping of the beam will occur. Additionally, rotation will not always be feasible, given certain sample and experimental setup geometries. Typical working distances for objective lenses used in micro-scale laser ablation are on the order of 1 cm, and so for samples on this size scale the appropriate rotation to account for non-orthogonal surfaces may not be possible without collision between the objective and sample, as in figure 1(b). Of course, besides these concerns, rotation protocols require extra translation stages, increasing experimental complexity.

A third solution, proposed here, is to transform the shape of the laser beam during machining without rotating the sample, using a digital micromirror device (DMD), a type of spatial light modulator. The corrected beam shape will take into account the local surface gradients, so that the projection on the surface will not appear stretched. Others have demonstrated a solution to a related problem, wherein a tilted beam output from the DMD results in a distorted image [14], and mask transformations are applied to recover the intended image on a surface orthogonal to the beam direction, which was intended for a fixed display purpose and hence did not involve closed-loop feedback for a changing surface orientation. Here, a beam optimised for output close to the normal of the DMD surface is used, and the surface at which the mask is imaged is tilted. Explicitly, the beam profile used for laser machining should be scaled by the cosine of the angle subtended by the incident beam vector and the sample surface normal, and the intensity of the beam at the mask increased by this same factor to account for the reduced mask area, whilst also taking into account the change to the Fresnel reflectivity. Beneficial to the technique is a depth of field great enough to encompass variations in sample height across an exposed region.

Whilst recent results have shown the fabrication of complex structures in a single laser pulse when using a DMD on an orthogonal surface [15, 16], and high resolution patterning when multiple exposures are used [17, 18] here we extend DMD beam shaping to the patterning of curved surfaces, without the use of rotation stages.

Although this work represents a proof-of-principle, size scales with applications in cell culture and, critically, biocompatibility for medical implants were chosen, which will be expanded upon in the results section. The desired surface patterning for the current work was an array of ~18 μm diameter circles, over the top side of a 3 mm diameter titanium sphere. A sphere was chosen in order to provide a continuous range in two axes of surface normal directions to correct for, hence providing a comprehensive test sample for this approach. Typically, micro-structured surfaces will show point-to-point lateral separations of uniform distances, and hence a regular angular spacing was chosen in order to approximate this in polar coordinates.
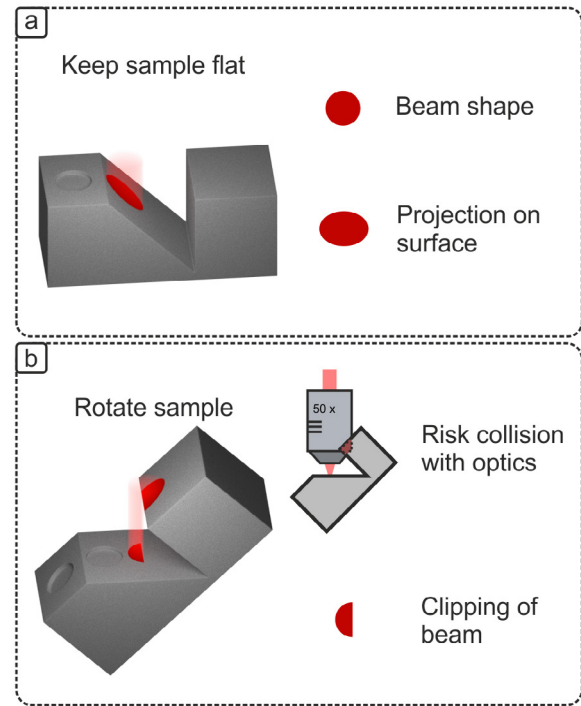
Figure 1. Laser machining over a non-planar sample can be achieved via (a) accepting a spatial stretching of the beam in some regions, or (b) rotation of the sample, which can be impractical due to experimental setup design, or be restricted by clipping of the beam. In this manuscript, we show a third approach via beam shaping without rotation.

This technique is a first proof-of-principle demonstration of using a spatial light modulator for laser machining of curved surfaces, and hence these values do not reflect the ultimate resolution limit of the technique, which will be determined, as usual, by the wavelength and numerical aperture of the system. Previous work on planar surfaces has already established that ~270 nm resolution is achievable [3].

In section 2, the experimental setup is described. In section 3, the closed-loop feedback components that were used enhance the positioning of the sample are discussed. Section 4 shows experimental results and analysis, and section 5 gives concluding remarks on the work.

2. Experimental setup

A Ti:sapphire amplifier was used to produce ultrashort (150 fs, 1 mJ, 800 nm wavelength) laser pulses, triggered on demand via external control of the cavity. While ultrashort pulses were used in this work, the method should be applicable to any combination of intensity, wavelength and pulse duration suitable to DMDs. The c.w. power handling of DMDs in the visible spectrum is around 25 W cm^{-2}, a value limited primarily by heat dissipation, while further considerations must be accounted for with pulsed sources [19]. The experimental setup is shown in figure 2.

Gaussian spatial intensity profile pulses were homogenised to 'top-hat' distributions using an AdlOptica 'π-shaper' (model 6_6), in order to ensure an equal intensity of exposure
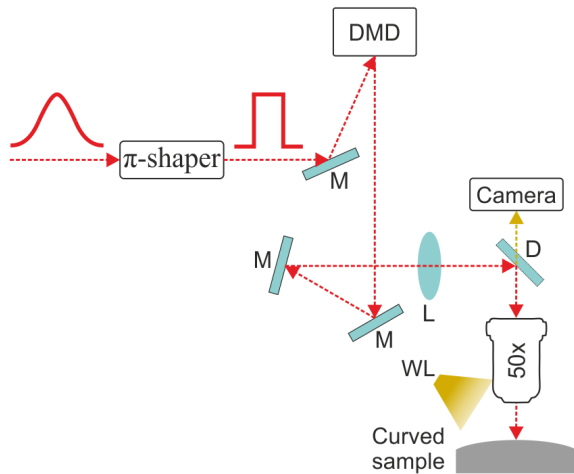
Figure 2. The experimental setup. The bitmap pattern displayed on the DMD acts as a variable exposure mask.

Figure 3. Schematic for laser machining circles over the top-half of a sphere, showing the result when (a) projecting a circle at a locally tilted region, resulting in an ellipsoid on the sphere surface and (b) projecting an ellipsoid an a locally tilted region, resulting in a circle as desired. Not included are focusing optics shown in figure 2, which have been omitted for clarity.

across the DMD. The MEMS mirrors of the DMD used in this work (DLP3000) were 7.64 μm wide, arranged in a diagonal-square lattice, such that centre-to-centre separations in the horizontal and vertical were 10.8 μm. The micro-mirrors had a reflectance of ~88% at 800 nm [19], while a glass layer in front of the active surface which contained an inert gas had a transmission of ~90% at 30° incidence [20]. By turning particular mirrors on or off, the surface of the DMD was enabled as a variable exposure mask at a fixed position in the setup, where bitmap patterns could be uploaded to position new masks on a millisecond timescale. The pulses diffracted into multiple orders at the DMD due to the periodic mirror layout, where each order contained sufficient spatial frequencies to image the overall mask shape. By taking advantage of the blaze angle, a single order ($m = 5$) containing ~30% of the incident pulse energy at an output angle of near 0° was isolated, and the energy within this diffracted order was used for machining. Light within this order was directed, via dielectric mirrors (M), through a collimating lens (L), and reflected from a dichroic mirror (D) through a 50× objective lens (Mitutoyo 50× NA = 0.42 infinity corrected) to the sample. The dichroic allowed viewing of the sample in real time, illuminated by a white light (WL) source, on a camera positioned above the objective. The sample was positioned via a 3-axis stage, with incremental single step sizes of ~1 μm and 50 mm travel in each direction.

For this first demonstration of laser machining of curved surfaces using a spatial light modulator, we show machining of circular patterns on the outside of the top half of a metal sphere, as shown in figure 3.

The effect of the surface gradient at each position was taken into account by modifying the spatial intensity profile of the beam from circular to a rotated ellipse, where the rotation and ellipticity were varied depending on the direction and magnitude of the local surface gradient, respectively. The long axis of any particular mask used here was 2.2 mm on the DMD surface, demagnified by a factor of 120× to 18 μm wide at the sample surface. The spacing between each projected beam shape was set to ensure a constant angular separation between
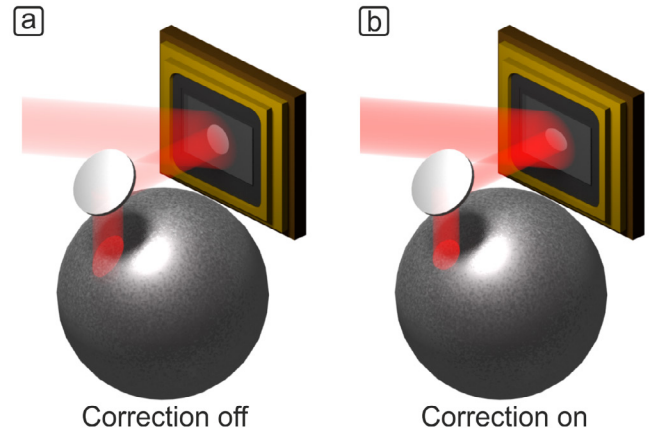
machined circles, hence ensuring equal nearest-neighbour distances between the machined features on the surface of the sphere. The laser intensity for each projected pulse shape was modified using a variable neutral density filter, and took into account the reduction in area (as compared to the area of the circle on the sphere surface) and the angular-dependent Fresnel reflectivity, assuming the local surface gradient over each 18 μm circular region to be uniform. The depth of field of the objective used was 1.6 μm, and the variation in sample height across the width of an exposed region would be difficult to account for with image projection-based techniques using fixed optics, which ordinarily will form an image in a fixed plane. Nonetheless, the sphere was translated in three axes, to ensure that the centre of the image plane of the projected beam profile always remained at the surface of the sphere, thus minimising the depth difference between the image plane and the sample surface at the edges of exposed regions.

Figure 4 shows the distribution of mask shapes required, as a function of Cartesian positions in a 'top-down' view of a 1 mm diameter sphere. A sphere diameter and range of azimuth different to those used in the experiments were used to enhance visual clarity of the diagram, though the ellipsoid shapes shown are typical of those used to produce the final results. The colour scale corresponds to the factor of increase in intensity required according to the reduced mask area and Fresnel reflections, where the central mask has been normalised to 1.

3. Closed-loop sample positioning

Maintaining the image plane of the exposure mask at the sample surface is always an important concern with image projection-based laser machining. However, this requirement presented additional technical considerations when working with a non-planar sample, particularly as the positional full-movement repeatability of the translation stages used was 10 μm, with 1 μm minimum step size. Consider the case of
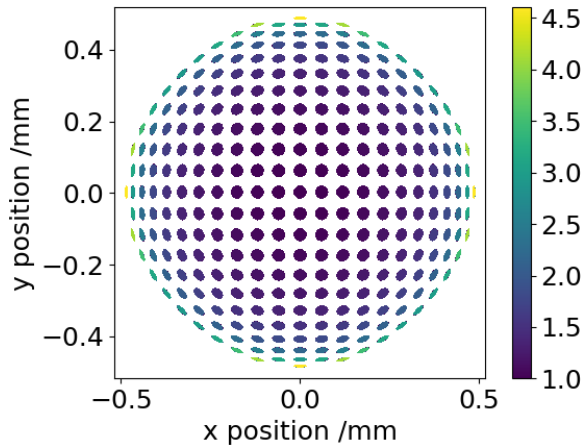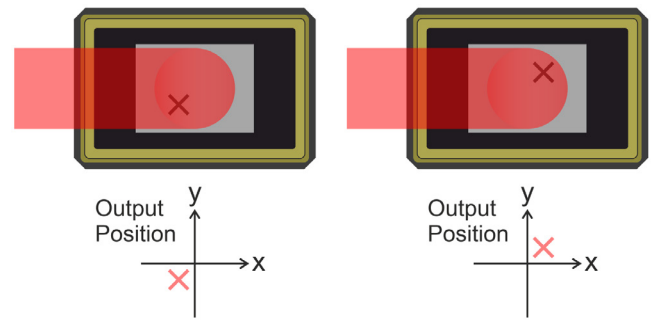
Figure 4. Schematic showing the required mask shape at each position, for laser machining circles in the top-half of a sphere, in order to project to a circle at the local surface gradient on a 0.5 mm radius titanium sphere sample. The color scale reflects the increase in intensity required as a result of Fresnel reflections and reduced mask area, where the central point has been normalised to a value of 1.

Figure 5. Two identical masks are translated on the DMD, in order to translate the beam at the sample. As the intensity was homogenised via a pi-shaper (model 6_6) prior to the DMD surface, as discussed in section 2, the intensities in the two beam profiles are identical.

Correction off   Correction on

Figure 6. Optical microscope images of an array of 5 by 5 'X' shapes laser machined into bismuth telluride, where each 'X' was produced via one exposure of the DMD. In (a) no positional correction was used, while in (b) both iterative translation stage corrections were made along with exposure mask repositioning on the DMD.

Figure 7. SEM images of (a) the single quadrant of the top-half of the sphere that was machined, (b) a higher magnification image of the topmost region, rotated for clarity, (c) a single machined circle from the top-most region at angle 0.04 rad.
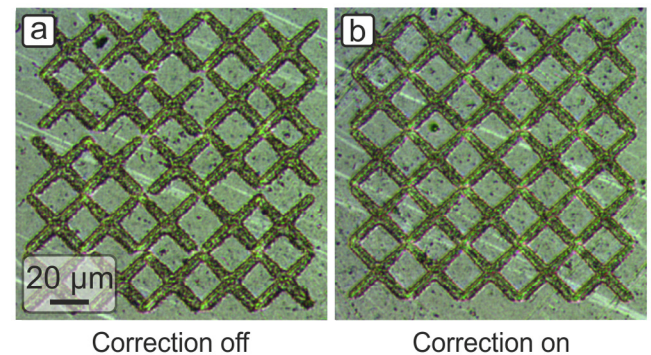
attempting to maintain the image plane at the sample surface of a 3 mm diameter sphere, at a deflection of $\pi/4$ from the vertical. At this point, a 10 μm lateral positional error will result in the sample surface being approximately 7 μm above or below the image plane. While this effect will be lessened near the top of the sphere, where the sample is locally orthogonal, it becomes increasingly prominent at greater local surface gradients. Even if the lateral repositioning could be assumed to be perfect, repeated translations in the vertical axis required to track the curved sample surface will accrue errors over time.

Prior to vertical repositioning, iterative lateral corrections were applied. The full field of view of the camera was on the order of 500 μm. As each sequential machining position separation was 30 μm or below, orthogonal to the camera viewing direction, a high proportion of sample features was visible before and after each sequential translation. This allowed for image shift detection algorithms, relying on phase correlation [21], a Fourier Transform-based technique. The camera view was used to evaluate the movement, for iterative feedback to update the stage position with down to 1 μm incremental movements. The largest errors encountered on the translation stages were at points where direction was reversed, where a backlash on the screw-driven motors as large as 10 μm was observed. Typically a single iteration of feedback was sufficient to correct positional errors, where the image shift detection informed the requested size of correction. In order to account for edge cases, where 10 μm of backlash was to be accounted for, but the sample position was only 1 μm from the correct position, up to 10 iterative corrective steps were allowed for any movement. Each iteration took ~1 s.
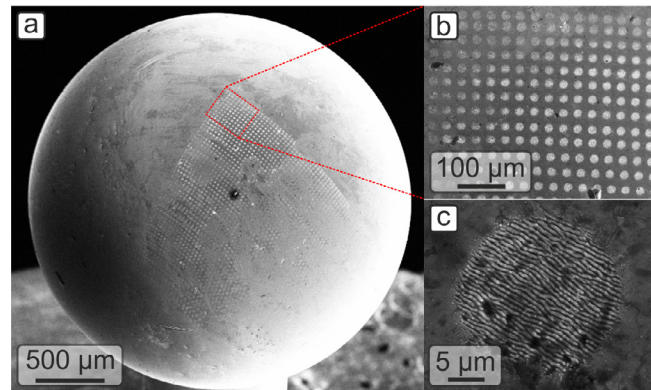
Finally, when the translations had been adjusted down to the 1 μm minimum step size of the stages, any error detectable via phase correlation compared to the previous position of machining was corrected for by translation of the mask on the DMD itself, as shown in figure 5.

Geometrically, each DMD pixel, (of size 7.64 μm), scaled down to ~92 nm at the sample. This meant that the centroid of intensity could be stepped laterally by 92 nm, however, the camera resolution, of ~350 nm, limited the accuracy of feedback that could be provided, and hence this was the limit of positional correction for the technique. Figure 6 compares
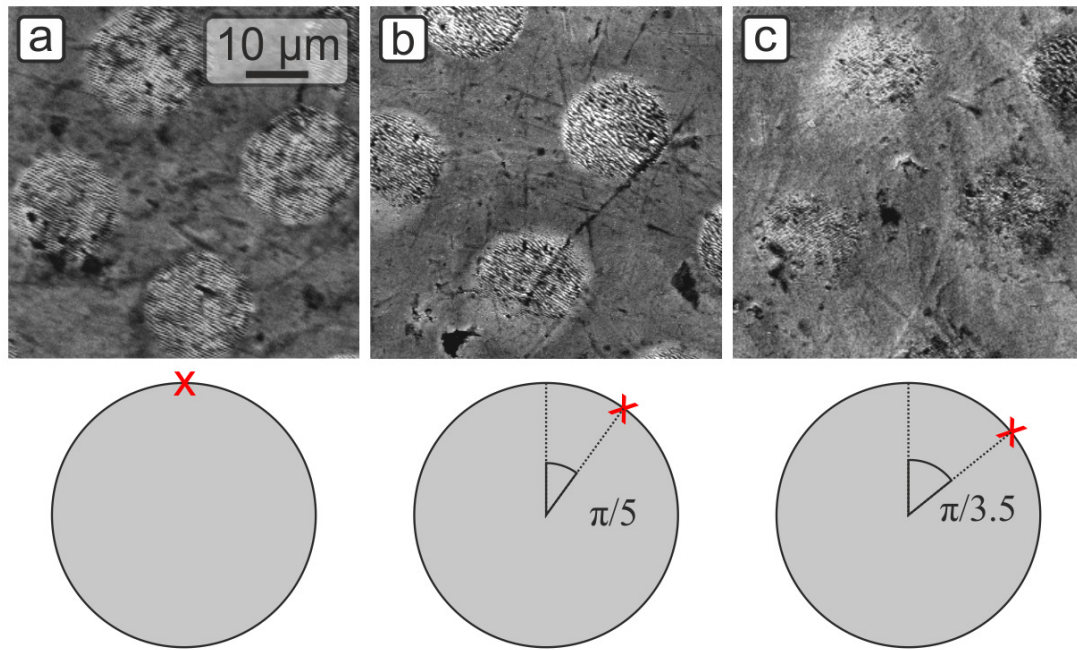
Figure 8. SEM images of (a) the top-most region (b) a region at an inclination of π/5, where some circles are poorly reproduced and (c) a region at an inclination of π/3.5, where all circles are poorly reproduced. Contrast has been adjusted on each image, for clarity.

the result of machining an array of 5 by 5 'X' shapes into a bismuth telluride surface (a material chosen for its low laser ablation threshold) with and without these two levels of lateral exposure position correction.

In order to correct for the vertical position, the live camera top-down view (as shown in figure 2) was used in conjunction with a focus-detection technique, which sought to iteratively adjust the vertical position, until high spatial frequencies were maximised on the camera image at the exposure position. High spatial frequencies present in the camera view correspond to minor scratches and defects in the sample surface being resolved, and hence corresponded to the image plane of the exposure mask coinciding with the surface of the sphere.

4. Experimental results and analysis

Titanium spheres of diameter 3.00 mm were used in this work, given the material's relevance to medical implants and the potential of surface patterning to enhance integration with the human body [22]. The semi-major axis of all ellipse masks displayed on the DMD were of length 100 pixels, which corresponded to machined circles of diameter 18 μm, a typical diameter observed for cells [23]. A full sample view, and higher magnification SEM results of the top-most regions are shown in figure 7. Inclinations in the range [0, π/2), and azimuths in the range [0, π/2] were tested, in steps of 0.02 rad, to produce local lateral nearest-neighbour separations of ~30 μm. The local vertical surface at an inclination of π/2 ensured that the technique must fail at some point, as this surface position was inaccessible with the set direction of the beamline. To machine each circle, between 20 and 100 pulses, with fluences ranging from 0.33 J cm^{-2} and 2.4 J cm^{-2}, were required, where pulse number and fluence per pulse were

varied in order to deliver an equal cumulative fluence when accounting for Fresnel reflections and reduced mask area, as described earlier. The total fluence at the sample was always 6.6 J cm^{-2}, i.e. equivalent to 20 sequential exposures at 0.33 J cm^{-2}, which was observed to produce a clear ablation depth of ~1 μm at the topmost position, consistent with titanium ablation depths found at similar combinations of fluence and pulse number [24], with other combinations of fluence and pulse number for a uniform total fluence deposition producing the same ablation depth across the curved surface. The resulting machined quadrant is shown in figure 7(a), while a close-up of the top-most machined points is shown in figure 7(b). The technique is shown to have machined all points successfully in this region. Figure 7(c) shows a single machined circle from this region, at an inclination angle of 0.04 rad, in which laser-induced periodic surface structuring (LIPSS) is apparent, a common result of repeated ultrafast laser exposures [25]. The LIPSS period observed here was ~620 nm, of the correct order of magnitude for relevance to the influence of cell response, and demonstrating an inherent degree of disorder which was found to be important in this field [5]. LIPSS periods have been found to be controllable via, among other factors, number of laser pulses [26].

Figure 8 shows high magnification SEMs of machined regions at various inclinations, in which figure 8(a) shows the topmost region of the sphere. While some pre-existing surface scratches affect the apparent quality of the machining, each circle has been reproduced correctly. Figure 8(b) shows a region at an inclination of π/5. At this point, distortions from a circular profile are evident at some points—note the blurred edges on the bottom and left-most circles shown. Figure 8(c) shows a region at an inclination of π/3.5, where all circles have been poorly reproduced.

Despite the limit of the technique observed in figure 8(b), it should be noted that the machined features have a near-uniform appearance; a lack of crisp edges to the features is the major difference to the circles machined at lower inclination angles. This uniformity suggests that the iterative focus and positioning algorithms were successful at these points. The poor edge quality of the features suggests that successful imaging of the intensity masks was not achieved at these positions, despite the correct sample position being tracked. This was likely linked to 1.6 μm depth of field of the objective used. At ~18 μm wide when viewed from the sample surface normal, an inclination angle of $\pi/3.5$ would imply a ~15 μm variation in absolute height across the targeted region. The lowering of ablation depth, even at the centre of machined features in figure 8(b), may have been due to optical filtering at the entrance to the objective, an effect observed previously when exposing DMD masks [16]. As greater inclination angles were targeted, increasingly oblate ellipsoid exposure masks were required. This, in turn, led to a greater proportion of intensity in higher spatial frequencies at the Fourier plane, which were filtered at the entrance pupil. In order to compensate for the discrepancy between image plane and the edge-positions of exposed regions, an appropriate phase-front tilt could be applied at the collimating lens position in figure 2, by mounting the collimating lens in a 2 D scanning system, or an objective with a greater depth of field could be used. While the scaling of input intensity at the DMD may be a limiting factor, from figure 4 it can be seen that in this case this value was only ~4, even in the most extreme cases, at angles above those where the tilt of the image plane was a greater concern. With a minimum fluence at the sample of 0.33 J cm^{-2}, a four-fold increase was not observed to cause damage to the DMD, where previous work has used ~10 times this intensity [27].

5. Conclusions

A combination of techniques has been used to demonstrate high-precision laser machining over a few mm-scale curved surface without the need for sample rotation. Applying transformations to the beam shape, via a DMD acting as a spatial light modulator, enabled the laser machining of near-identical circular features for up to $\pi/5$ deflections from the vertical on a 3.00 mm diameter titanium sphere. This technique is expected to be applicable for any intensity mask with features which, when transformed for the maximum deflection in local surface gradient of the sample, do not require resolutions below the optical limit of the setup. This work may have, in particular, biomedical applications, such as antimicrobial and hydrophobic/hydrophilic coatings as well as development of topographical cues for cell patterning, differentiation and function.

Acknowledgments

ORCID iDs

Daniel J Heath ● https://orcid.org/0000-0003-3566-1813
Benita S Mackay ● https://orcid.org/0000-0003-2050-8912
Ben Mills ● https://orcid.org/0000-0002-1784-1012

References

[1] Vorobyev A Y and Guo C 2006 Femtosecond laser nanostructuring of metals *Opt. Express* **14** 2164–9
[2] Ghany K A and Newishy M 2005 Cutting of 1.2 mm thick austenitic stainless steel sheet using pulsed and CW Nd:YAG laser *J. Mater. Process. Technol.* **168** 438–47
[3] Gamaly E G, Rode A V, Tikhonchuk B L T, Gamaly E G and Rode A V 2002 Ablation of solids by femtosecond lasers: ablation mechanism and ablation thresholds for metals and dielectrics *Phys. Plasmas* **9** 949
[4] Liang C, Wang H, Yang J, Li B, Yang Y and Li H 2012 Biocompatibility of the micro-patterned niti surface produced by femtosecond laser *Appl. Surf. Sci.* **261** 337–42
[5] Dalby M J, Gadegaard N, Tare R, Andar A, Riehle M O, Herzyk P, Wilkinson C D and Oreffo R O 2007 The control of human mesenchymal cell differentiation using nanoscale symmetry and disorder *Nat. Mater.* **6** 407–13
[6] Kietzig A M, Hatzikiriakos S G and Englezos P 2009 Ice friction: the effects of surface roughness, structure, and hydrophobicity *J. Appl. Phys.* **106** 024303
[7] Zorba V, Stratakis E, Barberoglou M, Spanakis E, Tzanetakis P, Anastasiadis S H and Fotakis C 2008 Biomimetic artificial surfaces quantitatively reproduce the water repellency of a lotus leaf *Adv. Mater.* **20** 4049–54
[8] Vorobyev A Y and Guo C 2009 Metal pumps liquid uphill *Appl. Phys. Lett.* **94** 224102
[9] Hwang T Y, Vorobyev A Y and Guo C 2011 Enhanced efficiency of solar-driven thermoelectric generator with femtosecond laser-textured metals *Opt. Express* **19** A824–9
[10] Singh N, Alexander D R, Schiffern J and Doerr D 2006 Femtosecond laser production of metal surfaces having unique surface structures that are broadband absorbers *J. Laser Appl.* **18** 242–4
[11] Heath D J, Mills B, Feinaeugle M and Eason R W 2015 Rapid bespoke laser ablation of variable period grating structures using a digital micromirror device for multi-colored surface images *Appl. Opt.* **54** 4984–8
[12] Vorobyev A Y and Guo C 2008 Colorizing metals with femtosecond laser pulses *Appl. Phys. Lett.* **92** 041914
[13] Tanvir Ahmmed K M, Grambow C and Kietzig A M 2014 Fabrication of micro/nano structures on metals by femtosecond laser micromachining *Micromachines* **5** 1219–53
[14] Messaoudi H, Thiemicke F, Falldorf C, Bergmann R B and Vollertsen F 2017 Distortion-free laser beam shaping for material processing using a digital micromirror device *Prod. Eng.* **11** 365–71
[15] Mills B, Feinaeugle M, Sones C L, Rizvi N and Eason R W 2013 Sub-micron-scale femtosecond laser ablation using a digital micromirror device *J. Micromech. Microeng.* **23** 35005
[16] Heath D J, Grant-Jacob J A, Eason R W and Mills B 2018 Single-pulse ablation of multi-depth structures via spatially filtered binary intensity masks *Appl. Opt.* **57** 1904–9

[17] Heath D J, Grant-Jacob J A, Feinaeugle M, Mills B and Eason R W 2017 Sub-diffraction limit laser ablation via multiple exposures using a digital micromirror device *Appl. Opt.* **56** 6398

[18] Heath D J, Rana T H, Bapty R A, Grant-Jacob J A, Xie Y, Eason R W and Mills B 2018 Ultrafast multi-layer subtractive patterning *Opt. Express* **26** 11928–33

[19] Texas Instruments 2012 Laser power handling for DMDs White Paper, January 2012

[20] Texas Instruments 2012 Wavelength Transmittance Considerations for DLP® DMD Window Application Report, May 2012

[21] Zitová B and Flusser J 2003 Image registration methods: a survey *Image Vis. Comput.* **21** 977–1000

[22] Anselme K and Bigerelle M 2005 Topography effects of pure titanium substrates on human osteoblast long-term adhesion *Acta Biomater.* **1** 211–22

[23] Ge J, Guo L, Wang S, Zhang Y, Cai T, Zhao R C H and Wu Y 3014 The size of mesenchymal stem cells is a significant cause of vascular obstructions and stroke *Stem Cell Rev. Rep.* **10** 295–303

[24] Mannion P T, Magee J, Coyne E, O'Connor G M and Glynn T J 2004 The effect of damage accumulation behaviour on ablation thresholds and damage morphology in ultrafast laser micro-machining of common metals in air *Appl. Surf. Sci.* **233** 275–87

[25] Bonse J, Rosenfeld A and Krüger J 2009 On the role of surface plasmon polaritons in the formation of laser-induced periodic surface structures upon irradiation of silicon by femtosecond-laser pulses *J. Appl. Phys.* **106** 104910

[26] Bonse J, Höhm S, Kirner S, Rosenfeld A and Krüger J 2016 Laser-induced periodic surface structures (lipss)—a scientific evergreen *Conf. Lasers Electro-Optics* vol 23 p STh1Q.3

[27] Mills B, Heath D J, Feinaeugle M, Grant-Jacob J A and Eason R W 2014 Laser ablation via programmable image projection for submicron dimension machining in diamond *J. Laser Appl.* **26** 041501